doi:10.1093/brain/awq168 Brain 2010: 133; 2462–2474 | 2462

BRAIN
A JOURNAL OF NEUROLOGY

SH3TC2, a protein mutant in Charcot–Marie–Tooth neuropathy, links peripheral nerve myelination to endosomal recycling

Claudia Stendel,[1,*] Andreas Roos,[2,*] Henning Kleine,[3,#] Estelle Arnaud,[4,#] Murat Özçelik,[1,#] Páris N. M. Sidiropoulos,[1,#] Jennifer Zenker,[4] Fanny Schüpfer,[4] Ute Lehmann,[3] Radoslaw M. Sobota,[5] David W. Litchfield,[6] Bernhard Lüscher,[3] Roman Chrast,[4] Ueli Suter[1] and Jan Senderek[1]

1 Institute of Cell Biology, Department of Biology, ETH Zürich, Zürich, Switzerland
2 Institute of Human Genetics, RWTH Aachen University, Aachen, Germany
3 Institute of Biochemistry and Molecular Biology, RWTH Aachen University, Aachen, Germany
4 Department of Medical Genetics and Service of Medical Genetics, University of Lausanne and Centre Hospitalier Universitaire Vaudois, Lausanne, Switzerland
5 Centre for Experimental Bioinformatics, Department of Biochemistry and Molecular Biology, University of Southern Denmark, Odense, Denmark
6 Department of Biochemistry, University of Western Ontario, London, Canada

*These authors contributed equally to this work.

#These authors contributed equally to this work.

Correspondence to: Dr Jan Senderek,
Institute of Cell Biology,
ETH Zürich,
Schafmattstr 18,
8093 Zürich, Switzerland
E-mail: jan.senderek@cell.biol.ethz.ch

Patients with Charcot–Marie–Tooth neuropathy and gene targeting in mice revealed an essential role for the *SH3TC2* gene in peripheral nerve myelination. *SH3TC2* expression is restricted to Schwann cells in the peripheral nervous system, and the gene product, SH3TC2, localizes to the perinuclear recycling compartment. Here, we show that SH3TC2 interacts with the small guanosine triphosphatase Rab11, which is known to regulate the recycling of internalized membranes and receptors back to the cell surface. Results of protein binding studies and transferrin receptor trafficking are in line with a role of SH3TC2 as a Rab11 effector molecule. Consistent with a function of Rab11 in Schwann cell myelination, *SH3TC2* mutations that cause neuropathy disrupt the SH3TC2/Rab11 interaction, and forced expression of dominant negative Rab11 strongly impairs myelin formation *in vitro*. Our data indicate that the SH3TC2/Rab11 interaction is relevant for peripheral nerve pathophysiology and place endosomal recycling on the list of cellular mechanisms involved in Schwann cell myelination.

Keywords: SH3TC2 / KIAA1985; Rab11; recycling endosome; Schwann cell myelination; Charcot-Marie-Tooth neuropathy

Abbreviations: CMT4C = Charcot–Marie–Tooth neuropathy type 4C; DAPI = diamidino-2-phenylindole dihydrochloride; DMEM = Dulbecco's modified Eagle's medium; GFP = green fluorescent protein; GST = glutathione *S*-transferase; PBS = phosphate buffered saline; PNS = peripheral nervous system; SDS–PAGE = sodium dodecyl sulphate–polyacrylamide gel electrophoresis; SH3TC2 = Src homology 3 domain and tetratricopeptide repeats 2

Received January 25, 2010. Revised May 8, 2010. Accepted May 14, 2010

Introduction

Myelin is a specialized membranous sheath, made up of ~70% lipids and 30% proteins. It is produced by two types of glia cells, oligodendrocytes in the central nervous system (CNS) and Schwann cells in the peripheral nervous system (PNS). Myelin surrounds nerve axons, allowing saltatory nerve conduction and ensuring maintenance of the axon at a long distance from the cell body (Griffiths *et al*., 1998; Lappe-Siefke *et al*., 2003; Nave and Trapp, 2008). The importance of myelin formation is illustrated by the severe neurological deficits seen in inherited and non-genetic demyelinating diseases of the CNS (e.g. multiple sclerosis and leukencephalopathies) and the PNS (e.g. autoimmune neuritis and hereditary neuropathies).

One condition associated with impaired myelination of the PNS is Charcot–Marie–Tooth disease type 4C (CMT4C) (LeGuern *et al*., 1996). CMT4C is an autosomal recessive form of hereditary motor and sensory neuropathies (Dyck *et al*., 1993) clinically presenting as distal muscle weakness and wasting, distal sensory deficits and prominent scoliosis (Kessali *et al*., 1997; Azzedine *et al*., 2006). Pathologically, CMT4C is characterized by layers of empty basal lamina encircling demyelinated and remyelinated axons, abnormal Schwann cell protrusions (Gabreels-Festen *et al*., 1999) and disorganization of the node of Ranvier (Arnaud *et al*., 2009).

We have previously shown that CMT4C is caused by mutations in the *SH3TC2* (*Src homology 3 domain and tetratricopeptide repeats 2*)/*KIAA1985* gene on chromosome 5q32 (Senderek *et al*., 2003). CMT4C is associated with both nonsense and missense mutations throughout the gene, and a strict genotype–phenotype correlation has not been established because of interfamilial and intrafamilial variability of clinical expression as well as marked allelic heterogeneity (Senderek *et al*., 2003; Azzedine *et al*., 2006; Colomer *et al*., 2006; Gosselin *et al*., 2008). *SH3TC2* encodes SH3TC2/KIAA1985, a novel protein of unknown function containing several motifs potentially involved in protein–protein interactions. However, no protein binding to SH3TC2 has been identified so far. Very recently, we found that a mouse model without a functional copy of the *Sh3tc2* gene developed a peripheral neuropathy that largely reproduced the human phenotype (Arnaud *et al*., 2009). Consistent with the tissue and the cell population involved in a demyelinating peripheral neuropathy, *Sh3tc2* is exclusively expressed in Schwann cells in peripheral nerves. SH3TC2 is tethered to cellular membranes through an N-terminal myristic acid anchor and localizes to the plasma membrane and a perinuclear membranous structure (Arnaud *et al*., 2009; Lupo *et al*., 2009) that corresponds to the endocytic recycling compartment (Arnaud *et al*., 2009). However, as the physiological function of the gene product, SH3TC2, has not yet been identified, the pathomechanism causing impaired PNS myelination in CMT4C patients and *Sh3tc2* knockout mice has so far remained unclear.

Here, we show that SH3TC2 is a novel effector of the small GTPase Rab11, a key regulator of recycling endosome functions. Neuropathy-causing missense mutations in *SH3TC2* disrupt this interaction. These data, together with the demonstration of the role of Rab11 in myelination, support the importance of the SH3TC2/Rab11 interaction for normal myelination.

Materials and methods

Animals

All experiments with animals followed protocols approved by the veterinary office of the Canton of Zurich, Switzerland. The generation of *Sh3tc2* knockout mice has been described previously (Arnaud *et al*., 2009). Genotypes were determined by polymerase chain reaction on genomic DNA derived from tail biopsies as reported earlier (Arnaud *et al*., 2009).

Plasmids

The generation of plasmids is outlined in the Supplementary material.

Cell culture and transfections

COS7, HEK293, HEK293T and RT4-D6P2T cells were cultured in Dulbecco's modified Eagle's medium (DMEM; Invitrogen) supplemented with 10% foetal calf serum (Invitrogen) and 2 mM glutamine (Invitrogen). Culture medium for Flp-In T-Rex 293 cells (Invitrogen) additionally contained 100 μg/ml Zeocin™ (Invitrogen) and 15 μg/ml blasticidine (Invitrogen). All transfections in this study were performed using Lipofectamine 2000 (Invitrogen) according to the manufacturer's instructions.

Flp-In T-Rex 293 cells that stably express inducible SH3TC2 fused to a C-terminal tandem affinity purification (TAP) tag (SH3TC2-C-TAP) or the TAP tag alone (C-TAP) were generated according to the manufacturer's instructions (Invitrogen). Hygromycin B (Invitrogen) at a concentration of 10 μg/ml was used for selection of stable cell clones. Cells were cultured with 15 μg/ml blasticidine and 10 μg/ml hygromycin B. In order to induce expression of SH3TC2-C-TAP or C-TAP, doxycycline (Sigma) was administered to the cells at a final concentration of 1 μg/ml for 20–24 h.

Generation of lentiviral stocks

For production of high-titre lentiviruses, HEK293T cells were transiently cotransfected with the pSicoR vector harbouring the complementary DNA of choice and the packaging constructs pMD2.G and psPAX2 (Addgene). Cell culture supernatant was collected after 48 and 72 h. The filtered supernatant was first centrifuged in an SW28 rotor (Beckmann Coulter) for 2 h at 21 000 r.p.m. at 11°C. Afterwards, the pellet was resuspended in DMEM/10% foetal calf serum and centrifuged again for 1 h at 16 000 r.p.m. at 4°C in a T60i rotor (Beckmann Coulter). The pellet was resuspended in 40 μl phosphate buffered saline (PBS), aliquoted and stored at −80°C.

Antibodies

Antibodies used in this study are described in the Supplementary material.

Tandem affinity purification

Flp-In T-Rex 293 cells stably expressing SH3TC2-C-TAP in a doxycycline-inducible fashion and a control cell line expressing the C-TAP tag alone (C-TAP) were used for purification of an SH3TC2 protein complex. The detailed protocol for tandem affinity purification has been described previously (Kleine *et al*., 2008).

Western blotting

Cultured cells were harvested, washed twice with PBS and lysed in lysis buffer (10 mM Tris–HCl, 5 mM EDTA, 150 mM NaCl, 1% Triton X-100) containing protease and phosphatase inhibitors (Sigma). Mouse and rat sciatic nerves were homogenized with a mortar and pestle in lysis buffer. Post-nuclear supernatants were boiled in sodium dodecyl sulphate (SDS) sample buffer (80 mM Tris pH 6.8, 10% glycerol, 2% sodium dodecyl sulphate, 0.002% bromphenol blue), resolved by sodium dodecyl sulphate polyacrylamide gel electrophoresis (SDS–PAGE) and electroblotted onto polyvinylidene fluoride membranes (Hybond-C; Amersham). Immunoblots were developed by incubation with appropriate antibodies followed by horse radish peroxidase- or alkaline phosphatase-chemiluminescence detection. Densitometry and quantification of protein levels were performed with Quantity One software (BioRad).

Coimmunoprecipitation

Transiently transfected HEK293 cells were harvested 24 h after transfection and the post-nuclear supernatant was pre-cleared with 30 µl of Protein G-Sepharose (GE Healthcare) at 4°C for 2 h. The supernatant was incubated with 30 µl of Protein G-Sepharose including 8 µg/ml of mouse anti-Myc, mouse anti-green fluorescent protein (GFP) or mouse anti-FLAG antibodies or mouse IgG. Immunoprecipitation was carried out at 4°C on a rotating wheel for 16 h. The precipitates were washed six times with cold lysis buffer and boiled in SDS sample buffer to elute protein complexes. The supernatants were processed using standard SDS–PAGE and western blotting procedures.

Glutathione *S*-transferase pulldown assays

In vitro translation of SH3TC2/Sh3tc2 and the generation of glutathione *S*-transferase (GST) or GST-Rab11 fusion proteins is described in the Supplementary material. *In vitro* translated SH3TC2/Sh3tc2 proteins (10 µl of standard reactions) were incubated for 1 h at 4°C with 50 µl glutathione-Sepharose beads coupled with GST or GST-Rab11 fusion proteins. The beads were washed four times with TNN (50 mM Tris pH 7.5, 250 mM NaCl, 5 mM EDTA, 0.5 % Nonidet-P40, 1 mM DTT) buffer before eluting proteins by boiling the beads in SDS sample buffer. Samples were resolved by SDS–PAGE followed by Coomassie Brilliant Blue staining and autoradiography.

Yeast two-hybrid assay

Protein interactions were assayed in yeast using a two-hybrid approach according to the manufacturer's protocol (Dualsystems Biotech). pLexA-SH3TC2 or pLexA-Lamin C were transformed into the NMY32 reporter strain together with pACT2-Rab11a using the lithium acetate method. Cells were plated on plates lacking tryptophane and leucine (TRP-, LEU-) to select for transformants. After 3 days of growth, five medium-size colonies for each condition were replated on selection plates lacking tryptophane, leucine and histidine (TRP-, LEU-, HIS-). After 3 days protein interactions were determined by growth of colonies. The results given are representative of at least three trials.

Immunofluorescence microscopy

Cells were fixed with 4% paraformaldehyde in PBS for 10 min at room temperature, washed in PBS and permeabilized with 0.1% Triton X-100 (Sigma). Fixed cells were blocked for 30 min with 10% goat serum in PBS containing 0.1% Triton X-100 before incubation in primary antibodies in blocking medium overnight at 4°C. Cells were washed in PBS and incubated with fluorescent secondary antibodies in blocking solution for 1 h at room temperature. After washing, cells were incubated with 4′,6′-diamidino-2-phenylindole dihydrochloride (DAPI) (Sigma) to visualize nuclei, washed again and mounted in Immu-Mount (Thermo Scientific). For Rab11, p230 and GM130 stainings, 0.05% saponin (Sigma) was used as detergent instead of Triton X-100. Images were acquired using either an AxioVert Observer D1 fluorescence microscope (Carl Zeiss) or a TCS SP1 laser scanning confocal microscope (Leica). Images were further processed using Photoshop software (Adobe).

Subcellular fractionation

Cells were harvested, washed twice in PBS and lysed in homogenization medium (0.25 M sucrose, 1 mM EDTA, 10 mM Hepes–NaOH, pH 7.4) including protease and phosphatase inhibitors. Iodixanol gradient solutions of 5, 10, 15, 20 and 25% were prepared from a 50% Optiprep (Gibco) solution. Solutions were layered in 950 µl fractions with 250 µl post-nuclear supernatant on the top in Ultra-Clear centrifuge tubes (Beckmann Coulter) and centrifuged in an SW55 rotor (Beckmann Coulter) at 35 000 rpm for 20 h at 4°C. After centrifugation, fractions were collected from the bottom by tube puncture and proteins were precipitated with trichloroacetic acid. Equal volumes of each fraction were analysed by SDS–PAGE and immunoblotting.

Rab11a transcript quantification

Analysis of *Rab11a* mRNA expression is described in the Supplementary material.

Transferrin receptor recycling assay

HEK293 cells were transfected with SH3TC2-GFP wild-type or SH3TC2-GFP harbouring CMT4C missense mutations. Cells transfected with GFP alone or GFP transfected cells additionally treated with 10 µM monensin [an inhibitor of transferrin receptor recycling (Stein *et al*., 1984)] were used as controls. Twenty-four hours after transfection, cells were starved for 4 h at 37°C in serum-free DMEM with 0.1% bovine serum albumin and subsequently incubated for 30 min in serum-free DMEM/0.1% bovine serum albumin containing 8.4 mg/ml transferrin-Alexa Fluor 647 (Invitrogen). Cells were washed with ice-cold PBS and chased in serum-free DMEM/0.1% bovine serum albumin containing 1 mg/ml unlabelled holo-transferrin (Sigma) at 37°C for different lengths of time. Cells were washed, acid-stripped (0.2 M Na_2HPO_4, 0.1 M citric acid) and trypsinized. Cells were fixed in paraformaldehyde for 20 min, pelleted and resuspended in PBS containing 2% foetal calf serum, 20 mM EDTA and 0.02 % NaN_3. The fluorescence intensity of cell bound transferrin was measured for 2000 GFP positive cells and the average intensities of the cell populations were calculated. Data acquisition was done on a FACSCalibur flow cytometer using CellQuest software (BD Biosciences). The experiment was repeated three times.

Surface reconstruction of recycling endosomes

COS7 cells were transfected with wild-type SH3TC2-FLAG, SH3TC2_N881S-FLAG or GFP. Cells were fixed with paraformaldehyde 24 h after transfection and stained with rabbit polyclonal anti-Rab11a and mouse monoclonal anti-FLAG antibodies, followed by fluorescently labelled secondary antibodies. *Z*-stacks in 0.122 μm intervals were taken for 100 transfected cells per condition (identified by FLAG staining or GFP fluorescence) with equal settings for zoom factor, laser intensity and pinhole. To estimate the surface of recycling endosomes, Rab11a positive surface areas were quantified with Imaris software (Bitplane) and corrected for cell size. The surface module of Imaris software was used for 3D reconstructions of recycling endosomes.

In vitro myelination

Preparation of dorsal root ganglia for dorsal root ganglion explant cultures, culture conditions and assessment of myelination are described in the Supplementary material.

Preparation and culture conditions of rat Schwann cells and dorsal root ganglion neurons for Schwann cell-dorsal root ganglion neuron co-cultures are described in the Supplementary material. Four days prior to adding Schwann cells to dorsal root ganglion neurons, Schwann cells were transduced by overnight incubation with the lentivirus of interest. Infected Schwann cells (200 000 per coverslip) were added and co-cultures were kept in C-medium (MEM; Invitrogen), supplemented with 10% foetal calf serum, 4 g/l D-glucose, 2 mM L-glutamine (Invitrogen), 50 ng/ml neural growth factor (Harlan) and 1% penicillin/streptomycin for 3 days. Myelination was induced over 10 consecutive days with C-medium supplemented with 50 μg/ml ascorbic acid (Sigma). Subsequently cultures were fixed for 20 min in 4% paraformaldehyde and for additional 15 min in ice-cold methanol at −20°C and blocked for 20 min with PBS containing 5% bovine serum albumin, 0.1% goat serum and 0.2% Triton X-100. Coverslips were incubated overnight at 4°C with primary antibodies in blocking solution. After additional washing steps in PBS, cultures were incubated with fluorescent secondary antibodies for 1 h at room temperature. Coverslips were washed again, incubated with DAPI and mounted with Immu-Mount. Myelinated segments were stained with a rat monoclonal anti-myelin basic protein antibody, followed by a Cy3-conjugated goat anti-rat IgG antibody. Neurons were detected with a mouse monoclonal anti-neurofilament antibody and a goat anti-mouse IgG antibody conjugated to Cy5. Transduction efficiency was monitored by GFP fluorescence. Myelination was evaluated as follows: ten fields per coverslip were randomly acquired (magnification 10×) and mean Cy3 fluorescence as an estimate of the number of myelin basic protein positive segments was calculated using ImageJ software (National Institutes of Health). Experiments were done in triplicate, at least three coverslips per condition were analysed for each experiment.

Statistical analysis

The data show the mean ± SEM. Statistical significance was determined using a two-tailed Student's *t*-test. Significance was set at $*P<0.05$, $**P<0.01$ or $***P<0.001$.

Results

Based on the observation that SH3TC2 contains several protein motifs (Src homology 3 domain domains and tetratricopeptide repeat repeats, Fig. 1A) known to mediate the formation of protein complexes (Senderek *et al*., 2003), we hypothesized that we might be able to deduce the function of SH3TC2 from already known functions of interacting proteins. As no proteins interacting with SH3TC2 were known and as the putative protein binding motifs in SH3TC2 did not allow prediction of a *bona fide* interaction partner, we decided to perform an unbiased screen for interacting proteins. We purified an SH3TC2 protein complex by means of tandem affinity purification from HEK293 cells, analysed the complex on an SDS gel and subjected the resulting protein bands to mass spectrometry. Among other proteins, we identified the small GTPase Rab11 as a protein potentially interacting with SH3TC2 (Fig. 1B and Supplementary Fig. 1A). Rab11 is a key regulator of recycling pathways from endosomes to the plasma membrane (Ullrich *et al*., 1996) and consists of two isoforms, Rab11a and Rab11b, which are encoded by different genes and mainly differ in their C-termini. Rab11a and Rab11b are differentially expressed (Sakurada *et al*., 1991; Lai *et al*., 1994) and may also be functionally different to some extent (Lapierre *et al*., 2003).

In order to confirm the results of the interaction screen, we expressed SH3TC2-Myc and GFP-Rab11a fusion proteins in HEK293 cells and performed coimmunoprecipitation in both directions. In addition to the co-precipitation of Rab11a along with SH3TC2, immunoprecipitation in the other direction showed that SH3TC2 could be coprecipitated with GFP-Rab11a as well (Fig. 1C). Results from GST pulldown and yeast two-hybrid experiments provided further evidence for the interaction between SH3TC2 and both Rab11 isoforms and showed that SH3TC2 binds directly to Rab11 (Fig. 1D and E; Supplementary Fig. 1B). However, we were not able to identify the particular protein region of SH3TC2 that mediates the interaction with Rab11 (Supplementary Fig. 2).

We have recently shown that both overexpressed proteins, SH3TC2 and Rab11a, colocalize with γ-tubulin and internalized transferrin in the perinuclear recycling endosome (Arnaud *et al*., 2009). We now expand our earlier findings by studying the distribution of SH3TC2-FLAG and endogenous Rab11a in epithelial cell lines (HEK293 and COS7) and a Schwann cell line (RT4-D6P2T). Since there was no antibody available against endogenous Sh3tc2, RT4-D6P2T cells that express *Sh3tc2* on the transcript level (data not shown) had to be transfected with the FLAG-construct as well. The localization of both proteins overlapped in the perinuclear region in all three cell lines (Fig. 2A). Moreover, strong colocalization was confirmed in consecutive optical sections along the microscope *z*-axis (Fig. 2B). Conversely, we observed no colocalization of SH3TC2 with marker proteins for other perinuclear organelles (Supplementary Fig. 3). In order to provide independent biochemical support for fluorescent microscopic findings, we subjected cultured cells overexpressing SH3TC2 to subcellular fractionation using Optiprep gradient centrifugation. Fractions were analysed for the presence of SH3TC2

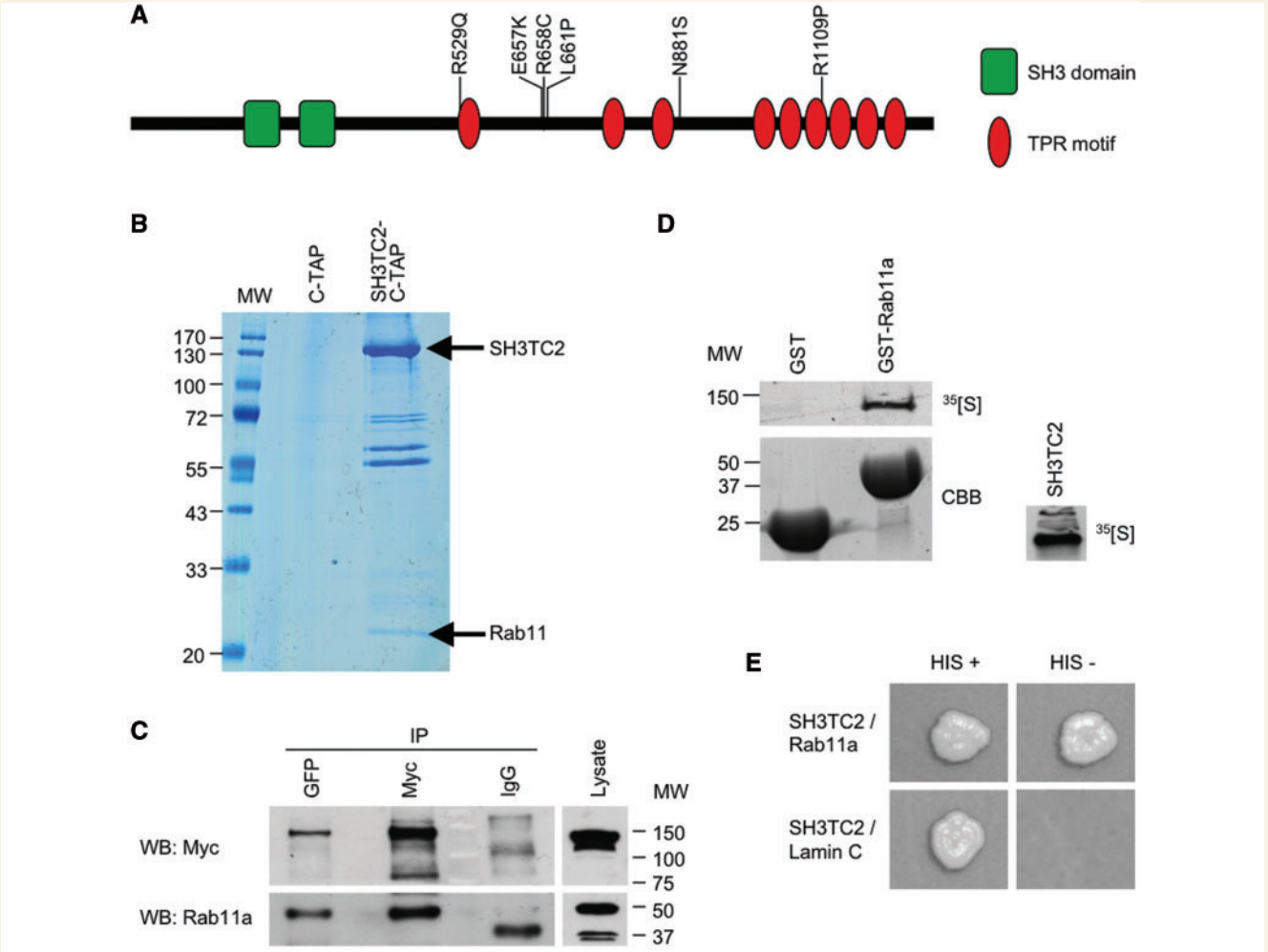

Figure 1 SH3TC2 interacts with the small GTPase Rab11. (**A**) Schematic drawing showing predicted domain structure of SH3TC2 and positions of CMT4C-associated missense mutations. Domains were predicted using Simple Modular Architecture Research Tool (SMART, http://smart.embl-heidelberg.de). (**B**) Identification of proteins complexing with SH3TC2 by tandem affinity purification. SH3TC2-C-TAP and C-TAP were purified from stably transfected Flp-In T-REx 293 cells and the interacting proteins were separated and visualized on a GelCode Blue-stained SDS gel. Resulting bands were analysed by mass spectrometry. (**C**) Coimmunoprecipitation of SH3TC2-Myc and GFP-Rab11a. HEK293 cells were transiently transfected with SH3TC2-Myc and GFP-Rab11a. Cells were lysed and an aliquot of the lysate was retained to analyse input protein levels (right). The remaining cell lysate was immunoprecipitated using mouse monoclonal Myc- and GFP-specific antibodies. Immunoprecipitation with mouse IgG was used as control. Protein complexes were resolved by SDS–PAGE and immunoblotted. SH3TC2-Myc was detected using a mouse monoclonal anti-Myc antibody, followed by a goat anti-mouse IgG antibody conjugated to horse radish peroxidase (upper left). GFP-Rab11a was detected using a rabbit polyclonal anti-Rab11a antibody, followed by a goat anti-rabbit IgG antibody conjugated to horse radish peroxidase (lower left). (**D**) GST pulldown of *in vitro* translated ^{35}[S]-SH3TC2 with Rab11a. Purified recombinant GST and GST-fused Rab11a were incubated with *in vitro* translated ^{35}[S]-SH3TC2. Bound labelled SH3TC2 was detected by autoradiography (upper left). GST proteins used in the pulldown were visualized by Coomassie staining (lower left). Autoradiographic detection of ^{35}[S]-SH3TC2 in the input proved successful *in vitro* translation (right). (**E**) Yeast-two-hybrid assay with SH3TC2 and Rab11a. pACT2-Rab11a was cotransformed into the yeast NMY32 reporter strain of *Saccharomyces cerevisiae* with pLexA-SH3TC2 or pLexA-Lamin C (as a negative control). Transformant viability is shown in the left panel (HIS+), while protein–protein interactions are indicated by growth of the transformants on media lacking histidine in the right panel (HIS−). CBB = Coomassie brilliant blue; IP = immunoprecipitation; MW = molecular weight; SH3 = Src homology 3; TPR = tetratricopeptide repeat; WB = western blot.

by immunoblotting and the profile was compared with the distribution of Rab11a. The bands for Rab11a were shown to overlap with the signal for SH3TC2 (Fig. 2C).

As there is increasing evidence that the development and maintenance of Schwann cells and the myelin sheath require endosomal sorting (Trapp *et al*., 2004; Simons and Trotter, 2007), we decided to follow the SH3TC2/Rab11 interaction further. As there were no published data on Rab11 expression in the PNS, we studied Rab11a protein levels in Schwann cell lines, primary rat Schwann cell cultures and sciatic nerves of rat and mouse by western blotting (Fig. 3A). We found that Rab11a was prominently expressed in cultured Schwann cells and in the PNS of

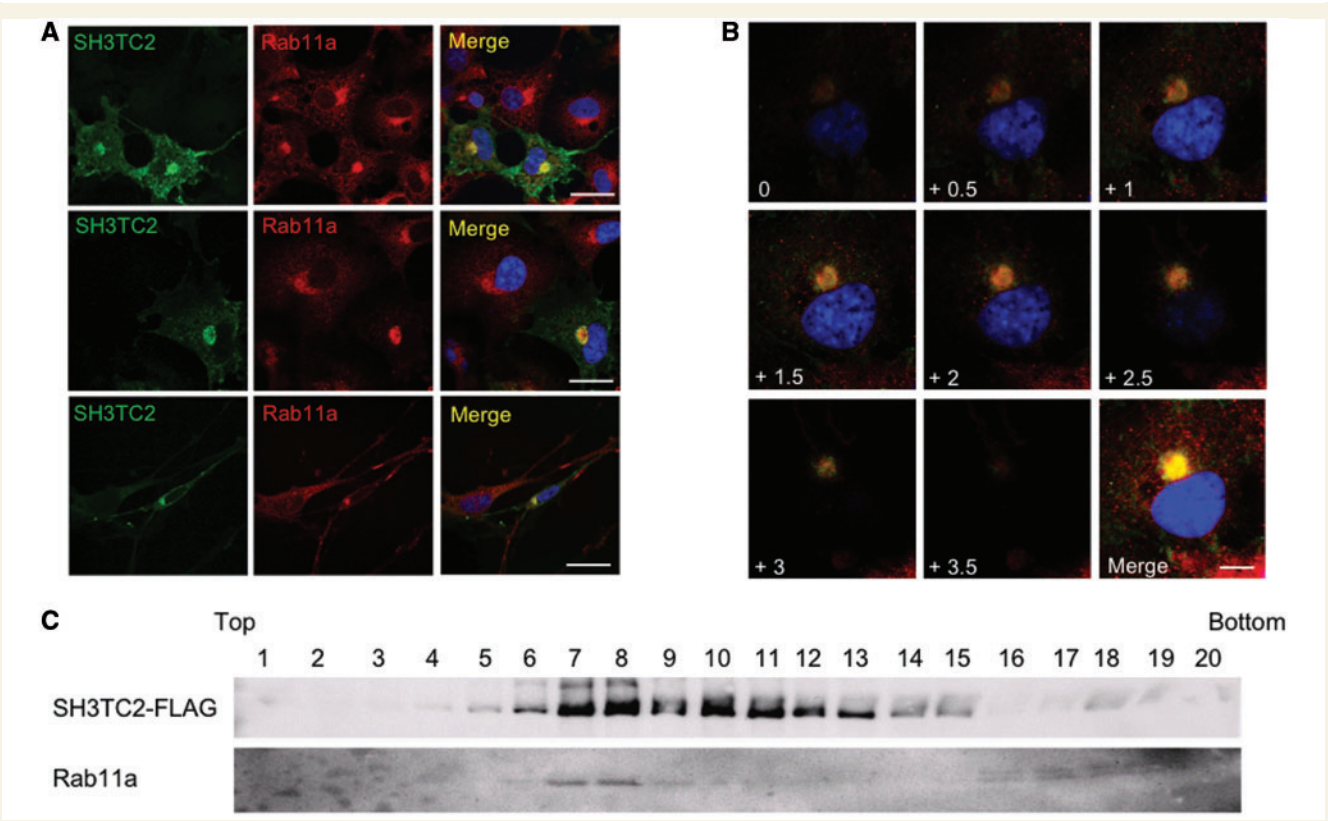

Figure 2 SH3TC2 and Rab11 localize to the same intracellular compartment. (**A**) Immunofluorescence studies of SH3TC2 and endogenous Rab11a in different cell lines using confocal microscopy. Cells were transiently transfected with SH3TC2-FLAG. The left column shows SH3TC2-FLAG in HEK29 (upper panel), COS7 (middle panel) and RT4-D6PT2 cells (lower panel), detected by a mouse monoclonal anti-FLAG antibody and an Alexa Fluor 488-conjugated goat anti-mouse IgG antibody. Endogenous Rab11a was visualized by a rabbit polyclonal anti-Rab11a antibody and a Cy3-conjugated goat anti-rabbit IgG antibody (middle column). Merged images are shown in the right column with nuclei stained with DAPI. Scale bars denote 20 μm. (**B**) Colocalization of SH3TC2 and Rab11a in consecutive optical sections of cells. COS7 cell were transiently transfected with SH3TC2-FLAG and stained with a mouse monoclonal anti-FLAG and an Alexa Fluor 488-conjugated goat anti-mouse IgG antibody (green) and a rabbit polyclonal anti-Rab11 antibody and a Cy3-conjugated goat anti-rabbit IgG antibody (red). A stack of confocal images (0.5 μm apart) from a double-labelled cell is shown with the nucleus stained with DAPI. A merged image of all confocal planes is show in lower right corner. Scale bar denotes 10 μm. **(C)** Detection of SH3TC2 and Rab11a in the same subcellular fractions. HEK293 cells were transiently transfected with SH3TC2-FLAG. Cells were lysed and post-nuclear supernatant was fractionated using a 5–25% Optiprep gradient. Equal amounts of fractions were resolved by SDS–PAGE and analysed by western blotting with a mouse monoclonal anti-FLAG and a mouse monoclonal anti-Rab11a antibody, followed by a goat anti-mouse IgG antibody conjugated to horse radish peroxidase. Twenty fractions were collected from lowest (top, lane 1) to highest (bottom, lane 20) density.

adult animals. Moreover, during the early stages of post-natal PNS development, Rab11a expression was strongly upregulated around post-natal day 10 (Fig. 3B), similar to the developmental expression profile of other proteins involved in myelination (Verheijen *et al*., 2003).

In order to explore whether binding of SH3TC2 to Rab11 is specific or whether SH3TC2 might promiscuously associate with different Rab GTPases, we performed GST pulldown assays with several proteins of the Rab family. No association was observed with Rab4a and Rab5a (associated with early endosomes) and Rab7a (associated with late endosomes) (Supplementary Fig. 4A). Having shown that wild-type SH3TC2 associates with Rab11 specifically we attempted to clarify whether the SH3TC2/Rab11 interaction is relevant for the pathogenesis of CMT4C. One obvious strategy to approach this intriguing question was to test CMT4C-causing SH3TC2 mutants (Fig. 1A) for their ability to associate with Rab11. We found that all tested amino acid substitutions related to missense mutations observed in patients with CMT4C disrupted the SH3TC2/Rab11a interaction (Fig. 4A). On the other hand, rat and mouse Sh3tc2 proteins bind to human Rab11a (Fig. 4B), although ~20% of amino acid residues are not conserved between the human and the rodent proteins (Fig. 4C, a multiple sequence alignment of human, mouse and rat SH3TC3/Sh3tc2 is shown in the Supplementary material). These findings establish that the disruption of the SH3TC2/Rab11 complex is a specific effect of CMT4C-causing missense mutations.

Next, we asked whether the SH3TC2/Rab11 interaction is dependent on the activation state of Rab11. Like all GTPases, Rab proteins cycle between an inactive (guanosine diphosphate-bound) and an active (GTP-bound) conformation. Interconversion

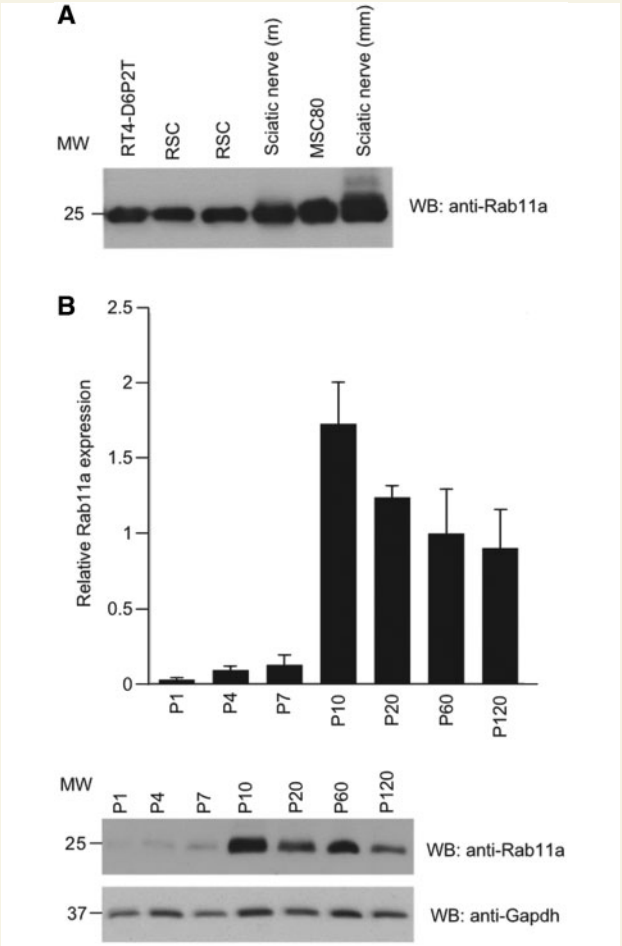

Figure 3 Expression of Rab11 in the peripheral nervous system. (**A**) Western blot analysis of different Schwann cell lines (RT4-D6PT2 and MSC80), primary rat Schwann cell (RSC) cultures and sciatic nerve lysates from adult mouse and rat. Rab11a was detected by using a mouse monoclonal anti-Rab11a antibody followed by a goat anti-mouse IgG (Fc) antibody conjugated to horse radish peroxidase. (**B**) Western blot analysis of Rab11a expression in the developing mouse sciatic nerve. Rab11a was detected by using the same antibodies as in **A**. To ensure similar loading, the membrane was probed with a mouse monoclonal anti-Gapdh antibody, followed by an alkaline phosphatase-conjugated goat anti-mouse IgG antibody. The blot shown is representative of three independent experiments. Quantification of these experiments is depicted in the graph showing Rab11a expression normalized against Gapdh levels. Error bars indicate ± SEM. MW = molecular weight; P = post-natal day; WB = western blot.

and accessibility of these two forms are temporally and spatially controlled by specific regulators (Stenmark, 2009). The GTP-bound, activated form of the GTPase associates with effector molecules through which it carries out its functions. We found that SH3TC2 interacts with the constitutive active GTP-bound Rab11_Q70L mutants, while there is no binding to the dominant negative guanosine diphosphate-bound Rab11_S25N mutants or to Rab11a_Q70L_I44E, a constitutively active mutant which has a second mutation in its effector domain abrogating effector binding (Wallace *et al*., 2002) (Fig. 5A and Supplementary Fig. 4B). Thus, the SH3TC2/Rab11 interaction is consistent with SH3TC2 functioning as a Rab11 effector.

Rab11 effectors have been shown to influence various functions of the recycling endosome, e.g. recycling of the transferrin receptor from endosomes back to the cell surface (Maxfield and McGraw, 2004). Assays for transferrin receptor recycling are commonly used as a paradigm to test recycling endosome functions (Sager *et al*., 1984). Such assays allow a quantitative assessment of the recycling rate of transferring receptor by measuring the amount of intact ligand that is retained in the cell (or has returned to the plasma membrane) upon time. Overexpression of wild-type SH3TC2 resulted in moderate slowing of transferrin recycling as compared with transferrin retention in cells transfected with CMT4C mutants or a GFP control vector (Fig. 5B and Supplementary Table 1). This suggests that wild-type SH3TC2 affects the rate of recycling along the receptor-mediated endocytosis pathway and this activity is largely absent in cells expressing SH3TC2 mutant proteins.

There is at least one known Rab11 effector, Rab11-FIP4, which causes a dramatic condensation of the recycling endosome (Wallace *et al*., 2002). Similarly, when SH3TC2 is expressed in transfected cells, not only does the endogenous Rab11a signal appear stronger, but the Rab11a-positive compartment appears to be more condensed in a perinuclear location (Fig. 2A and B). We quantified this effect by calculating the surface of Rab11a-positive endosomes in cells expressing wild-type SH3TC2 and the CMT4C-associated N881S mutant. The data we obtained confirmed that wild-type SH3TC2 condenses the perinuclear recycling compartment in a considerable proportion of transfected cells, while the N881S mutant had only a slight effect on recycling endosome morphology (Fig. 5C). This is in line with findings in teased fibres prepared from sciatic nerves of adult mice. The perinuclear Rab11 positive compartments are moderately less compact in Schwann cells lacking *Sh3tc2* than in the wild-type situation (Fig. 5D).

Since a number of Rab11 effectors, including Rab11-FIP2 and Rab11-FIP4, have been shown to be capable of homodimerization (Lindsay and McCaffrey, 2002; Wallace *et al*., 2002), we were interested to determine if SH3TC2 displays similar properties. Using coimmunoprecipitation of full-length SH3TC2, we were able to demonstrate that SH3TC2 can self-interact (Supplementary Fig. 4C).

We finally compared the Rab11 expression levels in sciatic nerves of *Sh3tc2* knockout mice and wild-type littermates, as it has been shown that Rab effectors can stabilize Rab-GTPases (Ganley *et al*., 2004). Indeed, we found that Rab11a protein levels were reduced in sciatic nerves of *Sh3tc2* knockout mice (Fig. 5E). Conversely, levels of *Rab11a* mRNA were unchanged in *Sh3tc2*-deficient mice, suggesting that Rab11a expression is differently regulated at the protein level in knockout and wild-type animals.

Our results presented so far open the intriguing possibility that a new Rab11 effector, SH3TC2, regulates Schwann cell myelination. In order to explore a potential effect of Rab11 and endosomal recycling on the formation of myelin sheaths in the PNS directly,

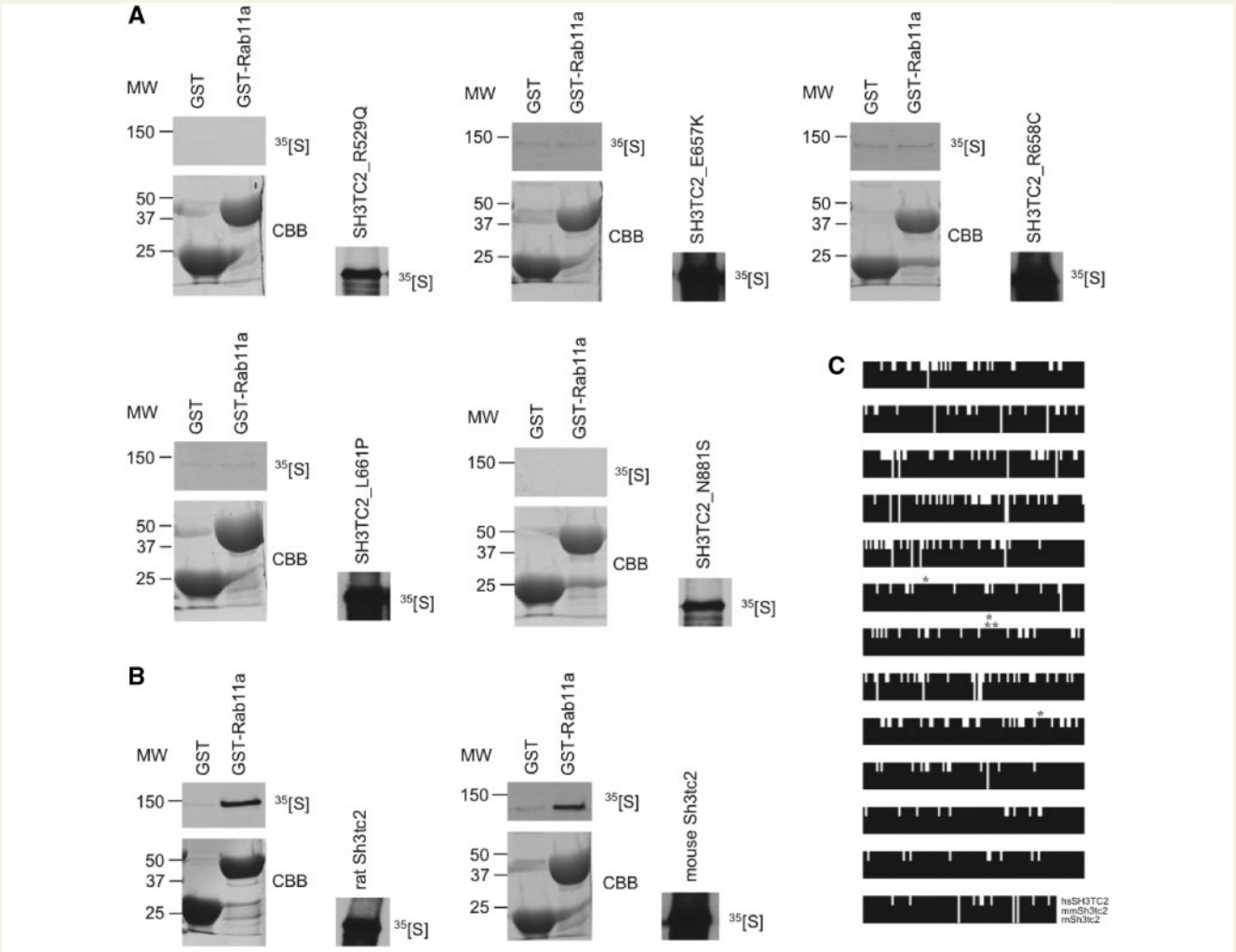

Figure 4 SH3TC2 binding to Rab11 is disrupted by CMT4C missense mutations. (**A**) GST pulldown experiments of different CMT4C-associated *in vitro* translated ^{35}[S]-SH3TC2 mutants with Rab11a. Purified recombinant GST and GST-Rab11a were incubated with five different *in vitro* translated ^{35}[S]-SH3TC2 missense mutants. Bound labelled SH3TC2 mutants were detected by autoradiography (upper left) and GST proteins present in the binding reaction were detected by Coomassie staining (lower left). Autoradiographic detection of ^{35}[S]-SH3TC2 mutants in the input proved successful *in vitro* translation (right). (**B**) GST pulldown of rodent Sh3tc2 with human GST-Rab11a. Purified recombinant GST and GST-Rab11a were incubated with *in vitro* translated mouse and rat ^{35}[S]-Sh3tc2. Bound labelled mouse and rat ^{35}[S]-Sh3tc2 were detected by autoradiography (upper left) and GST proteins present in the binding reaction were detected by Coomassie staining (lower left). Autoradiographic detection of rodent ^{35}[S]-Sh3tc2 in the input proved successful *in vitro* translation (right). (**C**) Multiple sequence alignment of human, mouse and rat SH3TC2/Sh3tc2 displaying conserved amino acids between species. CMT4C-related missense mutations affect amino acid residues in SH3TC2/Sh3tc2 that are conserved through evolution (indicated with asterisks). CBB = Coomassie brilliant blue; MW = molecular weight; Hs = human; mm = mouse; rn = rat.

we made use of two different established *in vitro* myelination systems.

Dorsal root ganglia were isolated from embryonic day 13.5 mice and infected with a lentivirus encoding dominant negative (S25N) or constitutively active (Q70L) forms of a Rab11a-GFP fusion protein or GFP alone. After 8 days in culture, myelination was induced by adding ascorbic acid to the medium. After 12 subsequent days of culturing, myelinated segments were visualized by myelin basic protein staining. Infection of dorsal root ganglia explants with a lentivirus encoding the dominant negative mutant of Rab11a impaired myelination compared with the control infected with a virus for GFP alone. On the other hand, infection with a lentivirus containing constitutively active Rab11a resulted in an increased number of myelinated segments (Supplementary Fig. 5A and B).

However, as lentiviral infection of dorsal root ganglia explants targets both Schwann cells and neurons, our data left open the question whether overexpression of Rab11 mutants in Schwann cells or neurons, or in both populations, was responsible for altered myelination. In order to dissect Rab11 effects in Schwann cells and neurons, we used primary rat Schwann cell-dorsal root ganglion neuron co-cultures. Primary rat Schwann cells were infected with Rab11a variants or GFP control lentivirus and were added to cultured mouse dorsal root ganglia. Following

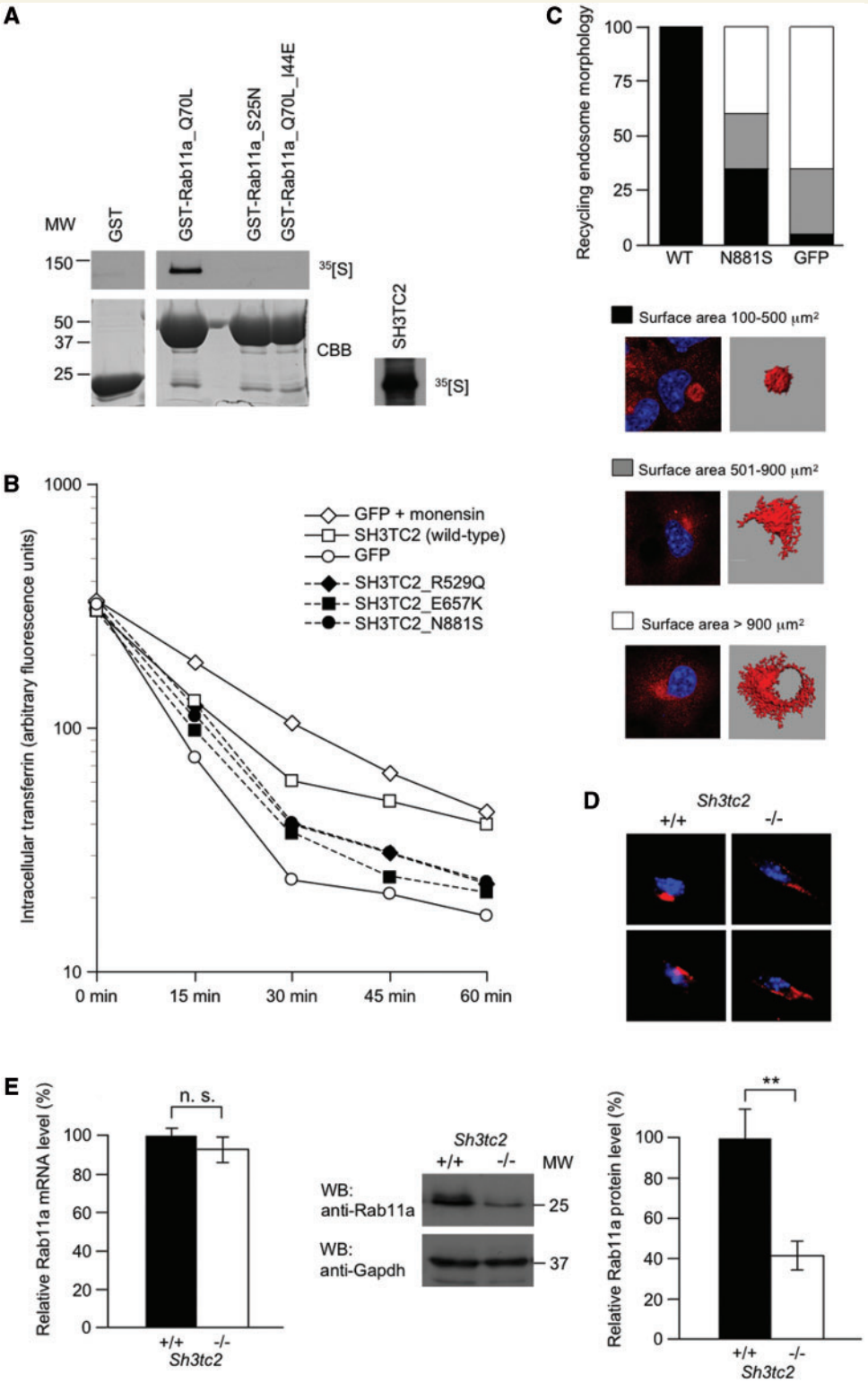

Figure 5 SH3TC2 is a potential new Rab11 effector. (**A**) GST pulldown of *in vitro* translated ^{35}[S]-SH3TC2 using Rab11a mutants interfering with nucleotide loading of the GTPase. GST and GST-Rab11a mutants [constitutively active, GTP bound (Q70L) and dominant negative, guanosine diphosphate bound (S25N)] were expressed as recombinant proteins and incubated with full length *in vitro* translated ^{35}[S]-SH3TC2. Binding of labelled SH3TC2 was detected by autoradiography (upper left). GST proteins present in the binding reaction were detected by Coomassie staining (lower left). Autoradiographic detection of labelled SH3TC2 in the input proved successful *in vitro* translation (right). (**B**) Kinetic analysis of transferrin recycling measured by fluorescent activated cell sorting. HEK293 cells were transfected with SH3TC2-GFP wild-type or SH3TC2-GFP harbouring CMT4C missense mutations. Cells transfected with GFP alone or GFP transfected cells additionally treated with 10 μM monensin [a potent inhibitor of transferrin receptor recycling (Stein *et al*., 1984)] were used as

Continued

induction of myelination by adding ascorbic acid, the amount of myelin production was assessed by myelin basic protein staining. Similar to dorsal root ganglion explant cultures, expression of the dominant negative mutant of Rab11a strongly impaired myelination, while expression of the constitutively active Rab11a resulted in moderately increased myelination (Fig. 6A and B). Altogether our data suggest that Rab11 controls Schwann cell myelination, most likely through regulation of SH3TC2 activity.

Discussion

We have previously shown that mutations in the *SH3TC2/Sh3tc2* gene cause demyelinating hereditary neuropathy in humans and mice (Senderek *et al*., 2003; Arnaud *et al*., 2009). The work presented here takes our understanding of the role of SH3TC2 in peripheral nerve demyelination to a new level: SH3TC2 acts as an effector of Rab11, a master regulator of recycling endosome functions (Maxfield and McGraw, 2004). In addition, we have shown that Rab11 itself is involved in the regulation of Schwann cell myelination *in vitro*, supporting the pathophysiological relevance of the observed SH3TC2/Rab11 interaction for peripheral nerves. Obviously, there is still the possibility that SH3TC2 can also influence myelination in a Rab11 independent manner. Potential candidates could be other proteins found in the SH3TC2 complex (Fig. 1A), whose role in the PNS and in Schwann cells has not yet been investigated.

Our findings directly lead to the question of how endosomal recycling might be involved in myelin sheath formation. Myelination requires dramatic changes in the cellular architecture of differentiating glia and a high degree of cell polarization that partitions the plasma membrane into distinct domains (Pfeiffer *et al*., 1993). Myelinating Schwann cells have at least five distinct membrane domains (Arroyo and Scherer, 2000; Simons and Trotter, 2007) that differ in their membrane lipid and protein composition. The outer (abaxonal) Schwann cell plasma membrane is specialized for extracellular interactions, while the inner (adaxonal) Schwann cell plasma membrane contains cell adhesion molecules (Previtali *et al*., 2001; Maurel *et al*., 2007; Spiegel *et al*, 2007). Compact myelin in the PNS is largely composed of lipids (mainly cholesterol and sphingolipids) and exhibits narrow lamellar spacings, mediated by homophilic adhesion molecules (Filbin *et al*., 1990). Membranes of the paranodal loops are enriched for junctional proteins that permit intra-Schwann cell junctions and Schwann cell–axon junctions (Fannon *et al*., 1995; Boyle *et al*., 2001). Finally, the membranes of Schwann cell microvilli contain ligands for axonal cell adhesion molecules and contribute to sodium channel clustering at the nodes of Ranvier (Eshed *et al*., 2005).

One crucial mechanism underlying establishment and maintenance of cellular polarity is differential sorting of proteins to distinct plasma membrane domains along the secretory and endosomal pathways (Keller *et al*., 2001; Kreitzer *et al*., 2003). Several lines of evidence indicate that protein transport and targeting play an important role in myelin membrane assembly. During myelination, Schwann cells establish specialized microtubule networks, suggesting increased rates of vesicle transport (Trapp *et al*., 1995; Kidd *et al*., 1996). Sorting in the trans-Golgi network partitions myelin proteins into separate transport vesicles (Trapp *et al*., 1995) that are targeted to distinct Schwann cell compartments. Similarly, in polarized epithelial cells, transfected Schwann cell proteins are distinctly transported, potentially reflecting the segregation of compact and non-compact myelin components (Minuk and Braun, 1996; Kroepfl and Gardinier, 2001; Maier *et al*., 2006). Finally, myelin proteins undergo endocytic recycling in oligodendrocytes (Winterstein *et al*., 2008), which are the myelinating glia cells in the CNS. However, molecular pathways regulating vesicular transport during myelination have remained largely unknown.

Figure 5 Continued
controls. The cells were incubated for 30 min with fluorescently labelled transferrin and then chased with an excess of unlabelled transferrin for the indicated lengths of time. The *y*-axis represents the intensities of the fluorescent signals in a log scale. Graphs represent the mean of three experiments. Values of data points ± SEM and significance levels are shown in Supplementary Table 1. (**C**) Effect of SH3TC2 on recycling endosome morphology. COS7 cells were transiently transfected with wild-type SH3TC2-FLAG, SH3TC2_N881S-FLAG or GFP. Endogenous Rab11a was labelled with a rabbit polyclonal anti-Rab11a antibody and a Cy3-conjugated goat anti-rabbit IgG antibody. Transfected cells were identified by GFP fluorescence or staining with a mouse monoclonal anti-FLAG and an Alexa Fluor 488-conjugated goat anti-mouse IgG antibody (not shown). One hundred cells were analysed per condition. Using stacks of confocal images (0.122 μm intervals) the Rab11a-positive surface was calculated and corrected for cell size to estimate the surface of the recycling endosome. Immunofluorescence pictures and 3D reconstructions show representative examples of each category of surface area. (**D**) Rab11a distribution in Schwann cells of *Sh3tc2* wild-type and knockout littermates. Teased nerve fibres were prepared from sciatic nerves of adult mice (at post-natal day 56). Rab11a was detected with a rabbit polyclonal anti-Rab11a antibody followed by a goat anti-rabbit IgG antibody conjugated to Alexa Fluor 594. Nuclei were stained with DAPI. (**E**) *Rab11a* mRNA and Rab11a protein levels in sciatic nerves of *Sh3tc2* wild-type and knockout littermates. *Rab11a* mRNA levels were obtained from cRNA microarray data from post-natal day 5 sciatic nerves of *Sh3tc2* wild-type and knockout littermates (R. Chrast and E. Arnaud, unpublished data). The quantification graph shows *Rab11a* mRNA levels normalized against *Gapdh* expression. For western blot analysis of sciatic nerves of wild-type and *Sh3tc2* knockout mice at post-natal day 5, Rab11a was detected with a mouse monoclonal anti-Rab11a antibody followed by a goat anti-mouse IgG (Fc) antibody conjugated to horse radish peroxidase. To ensure similar loading, the membrane was probed with a mouse monoclonal anti-Gapdh antibody, followed by an alkaline phosphatase-conjugated goat anti-mouse IgG antibody. The blot shown is representative of three independent experiments. Quantification of these experiments is depicted in the graph showing Rab11a expression normalized against Gapdh levels. Error bars indicate ± SEM. n.s. = not significant; $^{**}P < 0.01$. CBB = Coomassie brilliant blue; MW = molecular weight; P = post-natal day; WB = western blot; WT = wild-type.

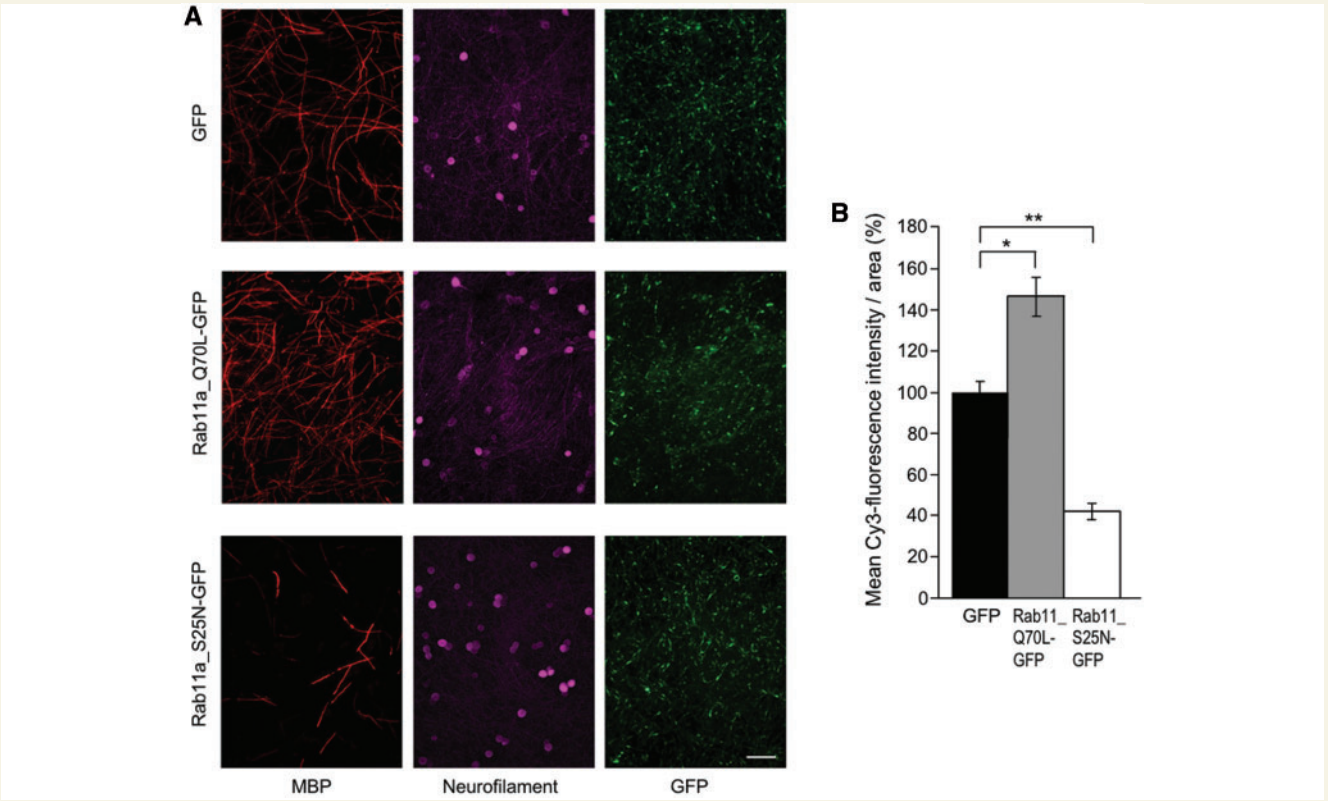

Figure 6 Rab11 regulates Schwann cell myelination in Schwann cell/neuron co-cultures. (**A**) Immunofluorescence studies of primary rat Schwann cells/mouse dorsal root ganglion neuron co-cultures after 12 days of myelination. Primary rat Schwann cells were either transduced with GFP (upper row) as a control, constitutively active Rab11a_Q70L-GFP (middle row) or dominant negative Rab11a_S25N-GFP (lower row). Myelinated segments were stained with a rat monoclonal anti-myelin basic protein antibody, followed by a Cy3-conjugated goat anti-rat IgG antibody (left column). Neurons were detected with a mouse monoclonal anti-neurofilament antibody and a goat anti-mouse IgG antibody conjugated to Cy5 (middle column). Transduction efficiency was monitored by GFP fluorescence (right column). Scale bar denotes 100 μm. (**B**) Quantification of myelin basic protein positive segments in Schwann cell/neuron co-cultures. Mean Cy3-fluorescence intensity per area was measured by ImageJ software and used as an estimate of the number of myelin basic protein positive segments. Mean Cy3-fluorescence intensity in control (GFP) infected Schwann cell/neuron co-cultures was set as 100% and compared with cultures expressing Rab11a_Q70L-GFP or Rab11a_S25N-GFP. Experiments were done in triplicate and at least three coverslips per condition were analysed in each experiment. Error bars indicate ± SEM; $*P<0.05$; $**P<0.01$.

By demonstrating the SH3TC2/Rab11 interaction, we provide evidence for a distinct molecular mechanism, which probably involves the recycling of cargos that are critical for Schwann cell myelination. *Sh3tc2*-knockout mice may be instrumental for isolating such cargos by analysing the expression levels and transport routes of Schwann cell surface receptors that are known to undergo endocytic recycling and to be involved in the regulation of myelination.

While our immunoprecipitation, GST pull down and yeast-two-hybrid data clearly demonstrated the SH3TC2/Rab11 interaction, we were unable to define a shorter linear motif in the SH3TC2 protein which supports the interaction with Rab11 (Supplementary Fig. 2). Moreover, single amino acid substitutions disrupting the SH3TC2/Rab11 complex are spread throughout the protein. One potential explanation could be that mutations of certain residues result in misfolding of SH3TC2, ultimately leading to the loss of interacting or stabilizing regions. However, we did not observe degradation of SH3TC2 mutants when expressed in cells (data not shown). Therefore, a more likely explanation would be that the mutated residues are all found on the surface of the protein, forming an extended Rab11-interacting domain. In line with this hypothesis, SH3TC2 does not contain a known Rab11-binding motif found in several other Rab11-interacting proteins (Prekeris *et al*., 2001). Obviously, the presence of this motif is not a prerequisite to function as a Rab11 effector, as it does not occur in all Rab11-interactors (Wu *et al*., 2005; Westlake *et al*., 2007). An extended interaction domain consisting of several tetratricopeptide repeat repeats (which are contained in SH3TC2 as well) has been reported to enable p67phox to interact with Rac1, a small GTPase of the Rho family (Lapouge *et al*., 2000).

In summary, the molecular dissection of the function of SH3TC2, a protein mutant in a comparatively rare genetic form of peripheral neuropathies, suggests a link between PNS demyelination and a key biological mechanism, endocytic recycling. The identification of Schwann cell and myelin proteins that undergo recycling endosome-dependent transport will extend and improve our understanding of the pathogenesis of peripheral neuropathies and will eventually provide us with a list of new candidate genes

and novel therapeutic targets. Assuming that endocytic recycling may assist morphogenesis of the myelin sheath by sorting and redirecting myelin components, it will be interesting to explore whether impaired endocytic recycling may be a common theme in demyelinating disorders of the PNS and maybe of the CNS as well.

During the preparation our manuscript, another article reporting the SH3TC2/Rab11 interaction and a potential effect of SH3TC2 on recycling endosome function was published (Roberts *et al*., 2010). While the data presented by Roberts *et al*. (2010) and by our group independently confirm that SH3TC2 is a new Rab11 effector molecule, we are going one step further and explore the role of Rab11 in Schwann cell myelination, demonstrating the relevance of the SH3TC2/Rab11 interaction for PNS pathology.

Acknowledgements

We thank Prof. M. McCaffrey (Department of Biochemistry, University College Cork, Ireland), Prof. L. A. Lapierre (Department of Surgery, Vanderbilt University Medical Center, Nashville, USA), Prof. B. Schlierf (Institut für Biochemie und Pathobiochemie, Friedrich-Alexander-Universität Erlangen-Nürnberg, Germany) and Prof. M. Zerial (Max Planck Institute for Molecular Cell Biology and Genetics, Dresden, Germany) for kindly providing us with Rab expression plasmids; and Prof. M. McCaffrey for her advice. J.S. is a Heisenberg fellow and C.S. a post-doctoral fellow of the Deutsche Forschungsgemeinschaft (DFG). A.R. received a PhD scholarship from RWTH Aachen University.

Funding

START program of RWTH Aachen University (to J.S.); the Interdisciplinary Centre for Clinical Research BIOMAT within the Faculty of Medicine; RWTH Aachen University (to J.S. and B.L.); the Swiss National Science Foundation (to R.C. and U.S.); the National Centre of Competence in Research; Neural Plasticity and Repair (to U.S.); Deutsche Forschungsgemeinschaft (to J.S. and B.L.).

Supplementary material

Supplementary material is available at *Brain* online.

References

Arnaud E, Zenker J, de Preux Charles AS, Stendel C, Roos A, Médard JJ, et al. SH3TC2/KIAA1985 protein is required for proper myelination and the integrity of the node of Ranvier in the peripheral nervous system. Proc Natl Acad Sci USA 2009; 106: 17528–33.

Arroyo EJ, Scherer SS. On the molecular architecture of myelinated fibers. Histochem Cell Biol 2000; 113: 1–18.

Azzedine H, Ravisé N, Verny C, Gabrëels-Festen A, Lammens M, Grid D, et al. Spine deformities in Charcot-Marie-Tooth 4C caused by SH3TC2 gene mutations. Neurology 2006; 67: 602–6.

Boyle ME, Berglund EO, Murai KK, Weber L, Peles E, Ranscht B. Contactin orchestrates assembly of the septate-like junctions at the paranode in myelinated peripheral nerve. Neuron 2001; 30: 385–97.

Colomer J, Gooding R, Angelicheva D, King RH, Guillén-Navarro E, Parman Y, et al. Clinical spectrum of CMT4C disease in patients homozygous for the p.Arg1109X mutation in SH3TC2. Neuromuscul Disord 2006; 16: 449–53.

Dyck PJ, Chance P, Lebo R, Carney JA. Hereditary motor and sensory neuropathies. In: Dyck PJ, Thomas PK, Griffin JW, Low PA, Poduslo JF, editors. Peripheral Neuropathy. 3rd edn., Philadelphia: W.B. Saunders; 1993. p. 1094–136.

Eshed Y, Feinberg K, Poliak S, Sabanay H, Sarig-Nadir O, Spiegel I, et al. Gliomedin mediates Schwann cell-axon interaction and the molecular assembly of the nodes of Ranvier. Neuron 2005; 47: 215–29.

Fannon AM, Sherman DL, Ilyina-Gragerova G, Brophy PJ, Friedrich VL Jr, Colman DR. Novel E-cadherin-mediated adhesion in peripheral nerve: Schwann cell architecture is stabilized by autotypic adherens junctions. J Cell Biol 1995; 129: 189–202.

Filbin MT, Walsh FS, Trapp BD, Pizzey JA, Tennekoon GI. Role of myelin P0 protein as a homophilic adhesion molecule. Nature 1990; 344: 871–2.

Gabreëls-Festen A, van Beersum S, Eshuis L, LeGuern E, Gabreëls F, van Engelen B, et al. Study on the gene and phenotypic characterisation of autosomal recessive demyelinating motor and sensory neuropathy (Charcot-Marie-Tooth disease) with a gene locus on chromosome 5q23-q33. J Neurol Neurosurg Psychiatry 1999; 66: 569–74.

Ganley IG, Carroll K, Bittova L, Pfeffer S. Rab9 GTPase Regulates Late Endosome Size and Requires Effector Interaction for Its Stability. Mol Biol Cell 2004; 15: 5420–30.

Gosselin I, Thiffault I, Tétreault M, Chau V, Dicaire MJ, Loisel L, et al. Founder SH3TC2 mutations are responsible for a CMT4C French-Canadians cluster. Neuromuscul Disord 2008; 18: 483–92.

Griffiths I, Klugmann M, Anderson T, Yool D, Thomson C, Schwab MH, et al. Axonal swellings and degeneration in mice lacking the major proteolipid of myelin. Science 1998; 280: 1610–3.

Keller P, Toomre D, Díaz E, White J, Simons K. Multicolour imaging of post-Golgi sorting and trafficking in live cells. Nat Cell Biol 2001; 3: 140–9.

Kessali M, Zemmouri R, Guilbot A, Maisonobe T, Brice A, LeGuern E, et al. A clinical, electrophysiologic, neuropathologic, and genetic study of two large Algerian families with an autosomal recessive demyelinating form of Charcot-Marie-Tooth disease. Neurology 1997; 48: 867–73.

Kidd G, Andrews SB, Trapp BD. Axons regulate the distribution of Schwann cell microtubules. J Neurosci 1996; 16: 946–54.

Kleine H, Poreba E, Lesniewicz K, Hassa PO, Hottinger MO, Litchfield DW, et al. Substrate-assisted catalysis by PARP10 limits its activity to mono-ADP-ribosylation. Mol Cell 2008; 32: 57–69.

Kreitzer G, Schmoranzer J, Low SH, Li X, Gan Y, Weimbs T, et al. Three-dimensional analysis of post-Golgi carrier exocytosis in epithelial cells. Nat Cell Biol 2003; 5: 126–36.

Kroepfl JF, Gardinier MV. Mutually exclusive apicobasolateral sorting of two oligodendroglial membrane proteins, proteolipid protein and myelin/oligodendrocyte glycoprotein, in Madin-Darby canine kidney cells. J Neurosci Res 2001; 66: 1140–8.

Lai F, Stubbs L, Artzt K. Molecular analysis of mouse Rab11b: a new type of mammalian YPT/Rab protein. Genomics 1994; 22: 610–6.

Lapierre LA, Dorn MC, Zimmermann CF, Navarra J, Burnette JO, Goldenring JR. Rab11b resides in a vesicular compartment distinct from Rab11a in parietal cells and other epithelial cells. Exp Cell Res 2003; 290: 322–31.

Lapouge K, Smith SJ, Walker PA, Gamblin SJ, Smerdon SJ, Rittinger K. Structure of the TPR domain of p67phox in complex with Rac-GTP. Mol Cell 2000; 6: 899–907.

Lappe-Siefke C, Goebbels S, Gravel M, Nicksch E, Lee J, Braun PE, et al. Disruption of Cnp1 uncouples oligodendroglial functions in axonal support and myelination. Nat Genet 2003; 33: 366–74.

LeGuern E, Guilbot A, Kessali M, Ravisé N, Tassin J, Maisonobe T, et al. Homozygosity mapping of an autosomal recessive form of demyelinating Charcot-Marie-Tooth disease to chromosome 5q23-q33. Hum Mol Genet 1996; 5: 1685–8.

Lindsay AJ, McCaffrey MW. Rab11-FIP2 functions in transferrin recycling and associates with endosomal membranes via its C-terminal region. J Biol Chem 2002; 277: 27193–9.

Lupo V, Galindo MI, Martínez-Rubio D, Sevilla T, Vílchez JJ, Palau F, et al. Missense mutations in the SH3TC2 protein causing Charcot-Marie-Tooth disease type 4C affect its localization in the plasma membrane and endocytic pathway. Hum Mol Genet 2009; 18: 4603–14.

Maier O, van der Heide T, Johnson R, de Vries H, Baron W, Hoekstra D. The function of neurofascin155 in oligodendrocytes is regulated by metalloprotease-mediated cleavage and ectodomain shedding. Exp Cell Res 2006; 312: 500–11.

Maurel P, Einheber S, Galinska J, Thaker P, Lam I, Rubin MB, et al. Nectin-like proteins mediate axon Schwann cell interactions along the internode and are essential for myelination. J Cell Biol 2007; 178: 861–74.

Maxfield FR, McGraw TE. Endocytic recycling. Nat Rev Mol Cell Biol 2004; 5: 121–32.

Minuk J, Braun PE. Differential intracellular sorting of the myelin-associated glycoprotein isoforms. J Neurosci Res 1996; 44: 411–20.

Nave KA, Trapp BD. Axon-glial signaling and the glial support of axon function. Annu Rev Neurosci 2008; 31: 535–61.

Pfeiffer SE, Warrington AE, Bansal R. The oligodendrocyte and its many cellular processes. Trends Cell Biol 1993; 3: 191–7.

Prekeris R, Davies JM, Scheller RH. Identification of a novel Rab11/25 binding domain present in Eferin and Rip proteins. J Biol Chem 2001; 276: 38966–70.

Previtali SC, Feltri ML, Archelos JJ, Quattrini A, Wrabetz L, Hartung H. Role of integrins in the peripheral nervous system. Prog Neurobiol 2001; 64: 35–49.

Roberts RC, Peden AA, Buss F, Bright NA, Latouche M, Reilly MM, et al. Mistargeting of SH3TC2 away from the recycling endosome causes Charcot-Marie-Tooth disease type 4C. Hum Mol Genet 2010. Advance Access published on December 22, 2009, doi:10.1093/hmg/ddp565.

Sager PR, Brown PA, Berlin RD. Analysis of transferrin recycling in mitotic and interphase HeLa cells by quantitative fluorescence microscopy. Cell 1984; 39: 275–82.

Sakurada K, Uchida K, Yamaguchi K, Aisaka K, Ito S, Ohmori T, et al. Molecular cloning and characterization of a ras p21-like GTP-binding protein (24KG) from rat liver. Biochem Biophys Res Commun 1991; 177: 1224–32.

Senderek J, Bergmann C, Stendel C, Kirfel J, Verpoorten N, De Jonghe P, et al. Mutations in a gene encoding a novel SH3/TPR domain protein cause autosomal recessive Charcot-Marie-Tooth type 4C neuropathy. Am J Hum Genet 2003; 73: 1106–19.

Simons M, Trotter J. Wrapping it up: the cell biology of myelination. Curr Opin Neurobiol 2007; 17: 533–40.

Spiegel I, Adamsky K, Eshed Y, Milo R, Sabanay H, Sarig-Nadir O, et al. A central role for Necl4 (SynCAM4) in Schwann cell-axon interaction and myelination. Nat Neurosci 2007; 10: 861–9.

Stein BS, Bensch KG, Sussman HH. Complete inhibition of transferring recycling by monensin in K562 cells. J Biol Chem 1984; 259: 14762–72.

Stenmark H. Rab GTPases as coordinators of vesicle traffic. Nat Rev Mol Cell Biol 2009; 10: 513–25.

Trapp BD, Kidd GJ, Hauer P, Mulrenin E, Haney CA, Andrews SB. Polarization of myelinating Schwann cell surface membranes: role of microtubules and the trans-Golgi network. J Neurosci 1995; 15: 1797–807.

Trapp BD, Pfeiffer SE, Anitei M, Kidd GJ. Cell biology of myelin assembly. In: Lazzarini RA, editor. Myelin biology and disorders. London: Elsevier academic; 2004. p. 29–48.

Ullrich O, Reinsch S, Urbé S, Zerial M, Parton RG. Rab11 regulates recycling through the pericentriolar recycling endosome. J Cell Biol 1996; 135: 913–24.

Verheijen MH, Chrast R, Burrola P, Lemke G. Local regulation of fat metabolism in peripheral nerves. Genes Dev 2003; 17: 2450–64.

Wallace DME, Lindsay AJ, Hendrick AG, McCaffrey MW. Rab11-FIP4 interacts with Rab11 in a GTP-dependent manner and its overexpression condenses the Rab11 positive compartment in HeLa cells. Biochem Biophys Res Comm 2002; 299: 770–9.

Westlake CJ, Junutula JR, Simon GC, Pilli M, Prekeris R, Scheller RH, et al. Identification of Rab11 as a small GTPase binding protein for the Evi5 oncogene. Proc Natl Acad Sci USA 2007; 104: 1236–41.

Winterstein C, Trotter J, Krämer-Albers EM. Distinct endocytic recycling of myelin proteins promotes oligodendroglial membrane remodeling. J Cell Sci 2008; 121: 834–42.

Wu S, Mehta SQ, Pichaud F, Bellen HJ, Quiocho FA. Sec15 interacts with Rab11 via a novel domain and affects Rab11 localization in vivo. Nat Struct Mol Biol 2005; 12: 879–85.